Textures and Microstructures, 1991, Vols 14–18, pp. 1055–1060
Reprints available from the publisher
Photocopying permitted by license only

ON THE IDEAL ORIENTATIONS OF ROLLING TEXTURES FOR FCC POLYCRYSTALS

Y. Zhou, K.W. Neale and L.S. Tóth *
Faculté des sciences appliquées
Université de Sherbrooke
Sherbrooke, Québec, Canada J1K 2R1

* Institute for General Physics
Eötvös University
1445 Budapest, P.O.B. 323, Hungary

ABSTRACT

The textures that develop during rolling are among the most important factors affecting the properties of rolled sheets, as well as their behaviour in subsequent forming processes. For FCC polycrystals, the main ideal orientations of rolling textures are cube, Goss, brass, copper, Taylor and S. The behaviour of these ideal orientations during rolling are investigated in this paper. Analytical and numerical results for the stress states, slip distributions, lattice rotation fields and orientation developments are obtained using a rate-sensitive crystal plasticity model. The rate-sensitive results are compared with those obtained from the classical rate-independent Bishop and Hill theory. Comparisons are also made with the experimental observations reported by Hirsch and Lücke.

1. INTRODUCTION

The textures that develop during rolling have been investigated for many years [1–6]. The main ideal orientations of rolling textures for FCC metals are found to be cube $\{001\} < 100 >$, G (Goss) $\{011\} < 100 >$, B (brass) $\{011\} < 211 >$, S $\{123\} < 412 >$ or $\{123\} < 634 >$ and C (copper) $\{112\} < 111 >$. In order to explain further the formation of rolling textures and the development of crystalline orientations during rolling, the behaviour of these ideal orientations, including T (Taylor) $\{4\,4\,11\} < 11\,11\,8 >$, are investigated in this paper using a rate-sensitive crystal plasticity model [7,8]. Analytical and numerical results for the stress states, slip distributions, lattice rotation fields and the development of orientations during rolling are obtained under three constraint conditions of deformation: plane strain compression (PSC), "lath" compression (LC), and "pancake" compression (PC).

The analysis shows that all the ideal orientations, except S, are highly symmetrical. In the limit of zero strain-rate sensitivity, the shear slips in the slip systems change continuously in the vicinity of these orientations. Four systems are active in the ideal positions with 4-equal or 2×2-equal slips. However, in the vicinity of the ideal orientations the stress states are not continuous – they change

suddenly from one vertex of the Bishop and Hill yield surface to the average of two or four vertices. The three dimensional rotation fields show that two fibres, which include the ideal orientations, exist. The formation of rolling textures depends on the behaviour of these two fibres during deformation. Comparisons with reported experimental observations indicate that the orientation changes in plane strain compression at small strains, in "lath" compression at intermediate strains and in "pancake" compression at large strains coincide with that of FCC metals with high stacking-fault energy during rolling.

2. CRYSTAL MODEL AND CONSTRAINT CONDITIONS

The rate-sensitive crystal model adopted in the present work is that employed by Tóth and co-workers [7,8]. The rate sensitivity of slip is expressed by a power-law relationship between the shear rate $\dot{\gamma}_s$ and resolved shear stress τ_s [10]:

$$\tau_s = \tau_0 \operatorname{sgn}(\dot{\gamma}_s)\left|\frac{\dot{\gamma}_s}{\dot{\gamma}_0}\right|^m = \tau_0 \frac{\dot{\gamma}_s}{\dot{\gamma}_0}\left|\frac{\dot{\gamma}_s}{\dot{\gamma}_0}\right|^{m-1} \tag{1}$$

where m is the strain-rate sensitivity index, τ_0 and $\dot{\gamma}_0$ are the reference shear stress and shear rate, respectively, assumed to be constant and equal for all slip systems in this analysis. The strain-rate tensor $\mathbf{D}$ associated with the Cauchy stress $\boldsymbol{\sigma}$ is given by the constitutive equation

$$D_{ij} = \frac{\dot{\gamma}_0}{2\tau_0^{1/m}} \sum_s (m^s_{ij} + m^s_{ji})\, m^s_{kl}\, \sigma_{kl} |m^s_{mn}\, \sigma_{mn}|^{1/m-1} \tag{2}$$

Here $\mathbf{m}^s = \mathbf{b}^s \times \mathbf{n}^s$ is the Schmid tensor for the slip system s. The vectors $\mathbf{b}^s$ and $\mathbf{n}^s$ are the unit slip direction and the unit slip plane normal for the slip system s in the deformed configuration, respectively. The lattice spin $\dot{\boldsymbol{\Omega}}$ can be determined from the relation

$$\dot{\Omega}_{ij} = \dot{\beta}_{ij} - \sum_s \frac{1}{2}(m^s_{ij} - m^s_{ji})\,\dot{\gamma}_s \tag{3}$$

where $\dot{\boldsymbol{\beta}}$ is the rigid body spin and the second term is the plastic spin. All geometrically possible slip systems are activated in rate-sensitive slip. The deviatoric stress components and shear rates are uniquely determined for a specified strain-rate state. The rate-insensitive response can be evaluated directly from these solutions as the limiting case of zero strain-rate sensitivity ($m \to 0$).

Here the laboratory coordinate system is defined by the X_1 and X_3 axes which correspond to the rolling and normal directions, respectively. Three types of constraint conditions are considered in the present work: plane strain compression (full constraints), "lath" compression (relaxed constraints), and "pancake" compression (relaxed constraints). For lath compression, the strain-rate component D_{13} is relaxed [11,12]. For the case of pancake compression, the grain shape is assumed to be very flat and two shear-rate components (D_{13} and D_{23}) are left free [11,12].

3. ANALYTICAL SOLUTIONS FOR THE IDEAL ORIENTATIONS

With the rate-sensitive model and the constraint conditions described above, the behaviour of the ideal orientations have been predicted analytically. The calculations are based on rate-sensitive slip in the 12 $\{111\} < 110 >$ slip systems of a FCC crystal (listed in [4]). The Euler angles of the considered ideal orientations

are: cube $(0°, 0°, 90°)$, G $(0°, 45°, 90°)$, B $(35.26°, 45°, 90°)$, S_1 $(56.79°, 29.21°, 63.43°)$, S_3 $(58.98°, 36.70°, 63.43°)$, C $(90°, 35.26°, 45°)$ and T $(90°, 27.37°, 45°)$. Table 1 gives the limiting solutions ($m \to 0$) for the stress states, slip distributions and lattice spins for the ideal orientations (except S). In Table 1, the stress states correspond to the boundary condition $\sigma_{11} = 0$.

Table 1 Limiting Solutions ($m \to 0$) for the Ideal Orientations.

Orientation	Constraint Conditions	Stress in Sample Axes (1-RD, 2-TD, 3-ND) (σ_{ij} =0, others)	Shear Rates in Active Slip Systems	Lattice Spin
Cube	PSC, LC, PC	$\sigma_{33}=2\sigma_{22}=-\sqrt{6}\tau_0$	$\dot{\gamma}_1=-\dot{\gamma}_4=-\dot{\gamma}_7=\dot{\gamma}_{10}=-\frac{\sqrt{6}}{4}D_{33}$	0
Goss	PSC, LC, PC	$\sigma_{33}=-\sqrt{6}\tau_0$	$\dot{\gamma}_7=\dot{\gamma}_9=-\dot{\gamma}_{10}=\dot{\gamma}_{12}=\frac{\sqrt{6}}{4}D_{33}$	0
Brass	PSC, LC, PC	$\sigma_{33}=\frac{5}{16}\sigma_{22}=-\frac{4}{3}\sqrt{6}\tau_0$ $\sigma_{12}=-\frac{2}{3}\sqrt{3}\tau_0$	$\dot{\gamma}_4=\dot{\gamma}_6=-\frac{1}{6}\sqrt{6}D_{33}$ $\dot{\gamma}_9=-\dot{\gamma}_{10}=\frac{1}{2}\sqrt{6}D_{33}$	0
Taylor	PSC	$\sigma_{33}=-5\sqrt{2}\sigma_{13}=-\frac{5}{2}\sqrt{2}\tau_0$ $\sigma_{22}=(-\frac{1}{4}\sqrt{6}-\frac{5}{4}\sqrt{2})\tau_0$	$\dot{\gamma}_6=-\dot{\gamma}_9=-\frac{3}{4}\sqrt{2}D_{33}$ $\dot{\gamma}_{10}=\dot{\gamma}_{11}=-\frac{1}{2}\sqrt{2}D_{33}$	0
Copper	LC, PC	$\sigma_{33}=\frac{3}{2}\sigma_{22}=-\frac{3}{2}\sqrt{6}\tau_0$	$\dot{\gamma}_6=-\dot{\gamma}_9=\dot{\gamma}_{10}=\dot{\gamma}_{11}=-\frac{3}{8}\sqrt{6}D_{33}$	$\frac{\sqrt{2}}{8}D_{33}$

3.1 Slip distributions and lattice rotations

Our analytical solutions show that, in the limit of zero strain-rate sensitivity, there are four activated slip systems with 4-equal or 2×2-equal slips for all the ideal orientations (except S), no matter what type of constraint condition is applied. The slip distribution is a consequence of the geometrical symmetry of these orientations. This equal-slip distribution pattern is a result of the basic feature of the rate-sensitive model, namely that equal resolved shear stresses imply equal slip rates. Such symmetrical slip distributions lead to no lattice rotations for the ideal orientations, except for the copper orientation in the two relaxed constraint cases. As seen in Eq. (3), the lattice rotation depends on the rigid body spin and plastic spin. It was pointed out by Tóth et al. [4] that the minimum number of slip systems necessary for zero plastic spin is four. Consequently, when rigid body rotations are absent (in full constraint cases, for example), at least four activated slip systems are required to maintain a constant orientation of a FCC grain. As mentioned above, four slip systems are activated for all the ideal orientations with equal shear rates, or two pairs of equal shear rates in the case of plane strain compression. Since rigid body rotation is present only for the copper orientation in the lath and pancake compression modes ($D_{13} \neq 0$), the slip distributions result in zero lattice spin for each of the ideal orientations, except copper.

The solutions also indicate that, for all the constraint conditions considered in the present work (full or relaxed constraints), the shears in the slip systems change continuously in the vicinity of the ideal orientations.

3.2 Stress states

In contrast to the continuous changes in the slip distributions near the ideal positions, the stress states change suddenly. As the sample axes move from the

vicinity of these orientations to the exact ideal orientations, the limiting ($m \to 0$) stress states jump from one vertex of the Bishop and Hill yield surface polyhedron to the average of two or four vertices. These steep changes in the stress states are due to the absence of high geometrical symmetry near the ideal positions. For example, there is one vertex in the vicinity of the Goss orientation under the condition of plane strain compression. If the same stress state is considered for the exact Goss position, a contradiction is found between the yield and slip conditions for some slip system (e.g., $\dot{\gamma}_1 = \dot{\gamma}_4$ but $\tau_1 = -\tau_4$), which violates the consistency law (if $\tau_k = \tau_0, \dot{\gamma}_k > 0$ and if $\tau_k = -\tau_0, \dot{\gamma}_k < 0$). Therefore, another stress vertex must contribute to the stress state to force $\dot{\gamma}_1 = \dot{\gamma}_4 = 0$ (or $|\tau_1| = |\tau_4| < \tau_0$). Due to the geometrical symmetry of this orientation, the stress state must correspond to the average of the two active stress vertices of the Bishop and Hill yield surface.

3.3 A new method to obtain rate-sensitive limiting solutions ($m \to 0$)

Comparing the limiting solutions of the rate-sensitive model with those of the Bishop and Hill theory for the case of full constraints, we find that the ambiguities of stress and slip distributions existing in the latter are resolved by the rate-sensitive model ($m \to 0$). When the prescribed strain-rate vector is perpendicular to a hyperplane of the Bishop and Hill yield surface, the stress state predicted by the rate-sensitive model in the limit $m \to 0$ is equal to the average of all the stress vertices of that particular hyperplane. For all the orientations considered in the present work, bi-equal or multi-equal (2, 4 or 8) slip is predicted by the rate-sensitive model ($m \to 0$).

These characteristics establish the connection between the limiting solution ($m \to 0$) of the rate-sensitive model and the Bishop and Hill rate-independent solutions, namely that the result of the rate-sensitive method ($m \to 0$) is one of the possible solutions of the Bishop and Hill theory. As a result, a new procedure can be proposed to obtain the limiting solution of the rate-sensitive model for symmetrical orientations as follows: First, the stress vertices and the corresponding activated slip systems are derived using the Bishop and Hill theory. Then, the stress state is taken as the average of all the yield surface vertices if two or more vertices are obtained. If the number of activated slip systems is greater than the number of the constraint conditions, we may assume that multi-equal slips occur, as long as the consistency law and the constraint conditions are not violated. Using the above procedure, the solutions obtained for all the ideal orientations would be identical to those listed in Table 1.

4. ROTATION FIELDS AROUND THE IDEAL ORIENTATIONS

The rotation fields in the vicinity of the ideal positions (within 10° orientation deviations) have been determined numerically using the rate-sensitive model and a very small value of strain-rate sensitivity ($m = 0.001$). The rotation fields reveal that, among the ideal orientations, only T and C are stable for the full and relaxed constraint conditions, respectively. Moreover, two fibres exist in the rotation fields: the α fibre (between G and B) and the β fibre (between $B - S_1'/S_3'/S_3 - T/C$). Here S_1' and S_3' differ from the S_1 and S_3 orientations by $\Delta\phi_1 \approx 9°$ and 6°, respectively. The shape of the β fibre depends on the boundary conditions. For plane strain compression, it consists of the brass, S_1' and Taylor orientations ($B - S_1' - T$). For lath compression it is formed by the $B - S_3 - C$, while for pancake compression it is defined by $B - S_3' - C$. During rolling, grain orientations move either directly into the β fibre, or first into the α fibre, then along the α to β, and finally towards the corresponding stable end orientations. Fig. 1 shows the schematic paths of the orientation changes under the boundary conditions considered. The rotation rates along the two fibres are very slow. As a

result, after large deformation few orientations could reach the end positions and most orientations remain distributed along the whole β fibre.

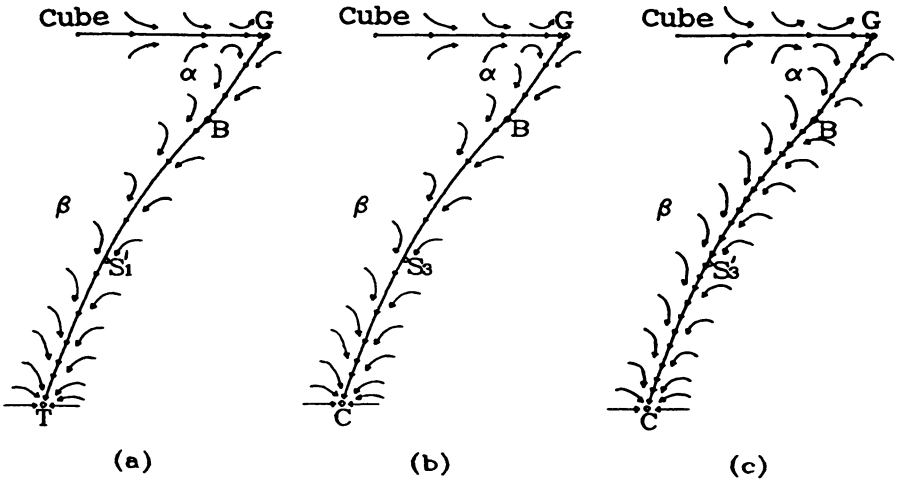

Figure 1 Schematic paths of the orientation development during: a) plane strain compression, b) lath compression, and c) pancake compression.

In addition to the different paths of texture formation, the boundary conditions also change the flow velocities of orientations along the α and β fibres. The movement along the α fibre is faster in plane strain compression (PSC) than in lath compression (LC) and pancake compression (PC). Under the conditions of PC, the rotations away from the brass position are quite slow. Accordingly, the brass orientation is metastable for this deformation mode. After grain orientations pass the S positions, their flow velocities are very small and almost the same for all the conditions considered. This implies that the S orientations are metastable during rolling. When grains reach the $\phi_2 = 50^\circ$ position, their movement becomes very slow in the PSC and LC deformation modes. This feature results from the pseudo-divergence of the rotation fields around $\phi_2 = 45^\circ$. On the other hand, the flow velocities of orientations towards the α and β fibres are strongly affected by the boundary conditions. Orientations rotate to the β fibre more slowly in the PSC mode than in the LC and PC modes. This implies that, in the latter two cases, most grain orientations can reach the α or β fibres at a lower degree of rolling deformation.

It is obvious from the above predictions that different constraint conditions result in different texture components after large deformation. For plane strain compression, the deformation texture is comprised of the $S_1' - T$ fibre. The relaxation of the strain-rate component D_{13} alters the texture so that it includes the main components $(S_3 - C)$. If both strain-rate components D_{13} and D_{23} are relaxed, the orientation flow rate changes, and the corresponding texture has the main components $(S_3' - C)$ as well as the weaker components brass and cube. The above observations imply that grain shapes can influence the formation of rolling textures since the relaxation of D_{13} and D_{23} is based on grain shape arguments.

We now compare the orientation change predictions described above with the experimental observations for FCC rolling textures reported by Hirsch and Lücke [3]. In general, the tendencies of the orientation changes during rolling predicted by the rate-sensitive model are in good agreement with measured rolling textures. An important observation is that orientation changes in plane strain

compression at small strains, in lath compression at intermediate strains, and in pancake compression at large deformations coincide with those of FCC metals with high stacking-fault energy (SFE). As the plane strain state deformation mode (full constraints) is applicable only at the beginning of rolling, the orientations of all FCC metals rotate to the α and β fibres with nearly equal density, independent of SFE. As deformation proceeds, the grains become flat so that the plane strain state cannot be maintained. In this case the orientation changes of high SFE metals gradually follow the behaviour of the lath and pancake modes. As a result, the α fibre gradually disappears and a slow movement along the β fibre leads to a stable end position near the copper orientation instead of the Taylor component. Because the flow velocities along the β fibre are very small, few orientations can reach their stable positions – most of them remain scattered along the β fibre even at high degrees of rolling. Consequently, the rolling texture is comprised mainly of the β fibre along which the three main components (brass, S and copper) can be found. According to the present predictions, the existence of the brass and S components is due to the metastability of the two orientations during pancake compression. At very large deformation, a peak density of orientation distribution would be formed at the S position. Meanwhile, the densities of the components B and C are increased.

8. CONCLUSIONS

From the present results it can be concluded that no ambiguities of the stress states or slip distributions exist in the limiting solutions of the rate-sensitive model ($m \to 0$). For symmetrical orientations, the limiting solutions are a sub-set of those predicted by the Bishop and Hill theory. Under the constraint conditions considered, a symmetrical stress state (the average of all the stress vertices involved) and symmetrical slip distribution (2, 4 or 8 slip systems each with the same shear rate) are the characteristic limiting solutions of the rate-sensitive model.

The formation of rolling textures is determined mainly by the behaviour of the α and β fibres during deformation. During rolling, orientations move either directly into the β fibre, or first into α, then along α to β, and they finally move along β towards their end stable positions. The different boundary conditions influence not only the composition of the β fiber but also change the flow velocities towards and along both fibres. This in turn leads to different final texture components at large rolling deformation.

REFERENCES

1. J. Grewen and G. Wassermann, *Acta Metall.*, **3**, 354 (1955).
2. J. Pospiech and K. Lücke, *Acta Metall.*, **23**, 997 (1975).
3. J. Hirsch and K. Lücke, *Acta Metall.*, **36**, 2863-2927 (1988).
4. L.S. Tóth, J.J. Jonas and K.W. Neale, *Proc. R. Soc. Lond.*, **A427**, 201 (1990).
5. S. Fuh and K.S. Havner, *Proc. R. Soc. Lond.*, **A422**, 193 (1989).
6. L.S. Tóth, J.J. Jonas, D. Daniel and R.K. Ray, *Metall. Trans.*, in press (1990).
7. L.S. Tóth, K.W. Neale and J.J. Jonas, *Acta Metall.*, **37**, 2197 (1989).
8. K.W. Neale, L.S. Tóth and J.J. Jonas, *Int. J. Plasticity*, **6**, 45 (1990).
9. J.F.W. Bishop and R. Hill, *Phil. Mag.*, **42**, 414 (1951).
10. R.J. Asaro and A. Needleman, *Acta Metall.*, **33**, 923 (1985).
11. P. van Houtte, *Proc. ICOTOM 6, p.*428, Tokyo, Iron and Steel Inst. of Japan (1981).
12. H. Honneff and H. Mecking, *Proc. ICOTOM 5*, **1**, Aachen, Springer, Berlin, 265 (1978).
13. U.F. Kocks, G.R. Canova and J.J. Jonas, *Acta Metall.*, **31**, 1243 (1983).